Focussed on: Computational Mechanics and Mechanics of Materials in Italy

Prediction of the pull-out strength of chemical anchors in natural stone

L. Contrafatto
University of Catania – Italy. Department of Civil Engineering and Architecture
loredana.contrafatto@dica.unict.it

R. Cosenza
University of Catania – Italy. Laboratory of Structural and Material Testing.
renato.cosenza@studium.unict.it

ABSTRACT. The applicability of some numerical models for the prediction of the failure mechanism and of the bearing capacity of post-installed threaded rods chemically anchored in basalt, sandstone and limestone is investigated, as well as the reliability of theoretical formulations conceived for concrete.
The numerical predictions, performed by means of engineering structural analysis software and advanced numerical codes, are compared with the results of an experimental research related to chemical anchors in natural stone. The minimum embedment depth for such fastening system is identified.

KEYWORDS. Adhesive anchor; Epoxy resin; Threaded rods; Sandstone; Basalt; Limestone.

INTRODUCTION

Masonry was in the past, and is, today, one of the most commonly used materials throughout the world for the construction of low rise buildings. The stonework is largely widespread in different countries and despite the variety of materials and techniques used, it has recurring problems regarding both the vulnerability to seismic actions and the applicability of reinforcement techniques. There are many techniques that can be implemented on masonry buildings. In particular, in the context of the retrofitting of existing buildings, a great development has been achieved with the use of anchoring systems. Chemical anchoring systems are commonly used in plain or reinforced concrete structures but also in structures in lightweight material, such as wood and brick, and in masonry constructions to rigidly couple different structural elements. A variety of metal elements are usually used, normally steel elements such as stirrups, reinforcement bars, threaded rods. The adhesive component of the system is generally resin.
Although the specific legislation on the architectural heritage does not allow the use of resin on historical and monumental buildings, but suggests the usage of special mortars, there exists a lot of cases in which the use of chemical anchoring is more suitable than mortar, especially in the case of anchoring systems on rocks or high resistance supports. Such is the case of all the masonry buildings that are not under a preservation order or listed buildings.
While a number of studies, both theoretical and experimental, concerns the behavior of concrete anchors, in terms of pull-out strength and anchor depth determination, as reported in [1-6], the lack of data concerning the behavior of chemical anchors in natural stone is incontrovertible and theoretical formulations in the literature valid for concrete are often not applicable, depending on the nature and quality of the stone type.

In the paper the application to chemical anchors in natural stone of theoretical models developed for anchoring systems in concrete is commented and the comparison between the theoretical results and the experimental data reported in [7] is performed. The anchor system under investigation consists in threaded rods glued to basalt, sandstone and limestone supports by means of epoxy resin. A set of experimental tests has been numerically simulated by using some models classically implemented in engineering structural software and the limit of these predictions is highlighted. Specifically, both axis-symmetric and 3D Finite Element discretisation of the anchor system have been performed. Drucker-Prager, Mohr-Coulomb or Concrete models were used to rule the stone constitutive behavior. A hardening plasticity model was assigned to the steel element. In 2D axis-symmetric simulations the resin was modeled linearly elastic, while in 3D simulations a bond slip model was introduced at the stone-rod interface. Moreover, the simulation of the pull-out test has been performed by the applications of an advanced software, belonging to the scientific research field, showing that only through a refined Finite Element modeling, based on enhanced formulation, a correct prediction both of the limit strength of the anchor and of the entire failure process can be obtained.

EXPERIMENTAL BEHAVIOUR OF THE ANCHORING SYSTEM

In [7] the minimum embedment depth for chemical anchoring of post-installed threaded rods in basalt, sandstone and limestone support has been experimentally determined. All the experiments took place at the Laboratory of Structural and Material Testing of Catania University.

Three types of natural stone samples were used in the tests, typical of eastern Sicily: sandstone squared blocks from the southeast Sicily (Palagonia sandstone) all of size 15x25x45 cm^3, basalt irregular blocks coming from a local quarry in the region of volcano Etna (Etna basalt), with dimensions ranging between 20x20x40 cm^3 to 30x40x60 cm^3, limestone blocks of quite irregular shape from the region of the mountain chain of Nebrodi and dimensions ranging between 20x30x40 cm^3 to 40x40x60 cm^3. The material data obtained by the mechanical characterization are reported in Table 1.

	Basalt	Limestone	Sandstone
Uniaxial compressive strength [N/mm^2]	500	220	20
Young Modulus E [N/mm^2]	50000	19616	12309
Density [kN/mm^3]	30.0	26.0	14.3

Table 1: Mechanical properties of the rocks

Threaded steel rods were unmarked, 4.6 class (tensile strength 400 N/mm^2 and yield strength 240 N/mm^2, verified by performing uniaxial tensile tests.

The HIT-RE 500 epoxy resin of the company Hilti was used as bonding agent, specifically designed for fastening into solid materials such as concrete, grout, stone or solid masonry. It is a high strength, two part epoxy adhesive composed by Component A (Epoxy resin, filler material) and Component B (hardener amine base, filler material).

The drilling of each rock sample was performed by column drill, with a hole diameter always 4 mm larger than the rod diameter, considering an efficient thickness of resin of 2 mm all around the rod, as usually recommended in these applications. Hole cleaning was carried out using compressed air and specific brushes to allow the optimal adhesion between the resin and the stone material. The epoxy resin was injected into the hole accompanied by the immediate insertion of the rod by screwing.

The effect of the embedment length on the pull-out strength of the steel rods chemically bonded into the three types of rock blocks was investigated for three embedment depths (3, 5 and 10 times the bar diameter) and three nominal diameter (10 mm, 14 mm, 20 mm).

The experimental tests consisted of applying a static pull-out force to the bar chemically bonded in the stone specimen by means of a hydraulic hollow cylinder FPT CRM-30/100 and measuring the intensity of the force by means a HBM MGC Plus data acquisition system. The triangular reaction frame with height-adjustable feet in Fig. 1(b), bearing on the stone block, was used as a base for the hollow cylinder, because stone blocks had irregular faces. Moreover the device had the role of maintaining the zone possibly interested by crisis mechanism free from confinement.

Eighty-one tests were performed. Each test was labelled by using a 4-fields alphanumeric code. The first alphabetic field identifies the stone type on which the experiment was done. A: Palagonia sandstone. B: Etna basalt. C: Floresta

limestone. The second numeric field identifies the diameter of the bar. The third numeric field identifies the embedment depth L of the bar. The last numeric field identifies the number of the sample for each series. Typically 3 samples in each series were tested.

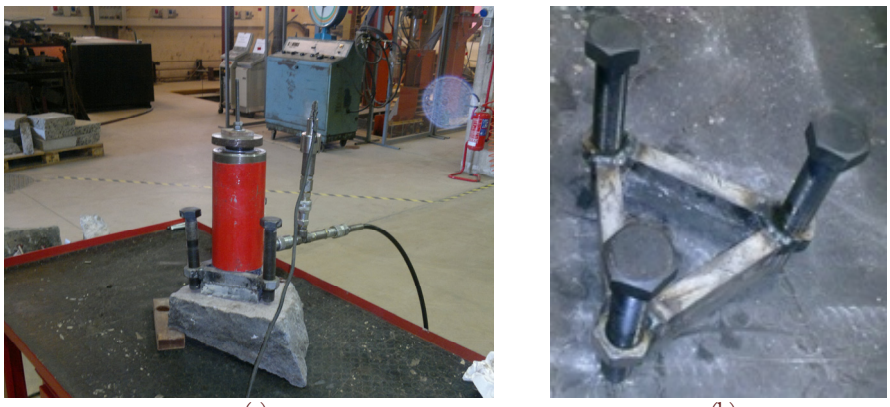

(a) (b)

Figure 1: Testing apparatus (a) and triangular reaction frame (b).

The failure mechanism of anchors in basalt and limestone was typically the yielding of the bar for an embedment length equal to five or ten times the diameter (see Fig. 2).

(a) (b)

Figure 2: Typical failure mechanisms in the case L=10ϕ. Basalt test B-10-10-1 (a) and limestone test C-14-10-2 (b).

Only for the length of anchor L=3ϕ the breaking process exhibited the formation of a stone cone, eventually coupled with sliding at the rock/resin interface (see Fig. 3(a)). On the contrary, in the case of sandstone, for each diameter and anchor length the failure was accompanied by the formation of a stone cone (see Fig. 3(c)).

(a) (b) (c)

Figure 3: Typical failure mechanisms in the case L=3ϕ. Basalt test B-10-3-2 (a) Limestone test C-14-3-2 (b) Sandstone test A-14-3-3(c)

Fig. 4, 5 and 6 report the experimental curves for the three rod diameters ϕ =10 mm, ϕ =14 mm, ϕ =20 mm respectively, with the different stones and embedment lengths.
A comprehensive report of the experimental results can be found in [7].

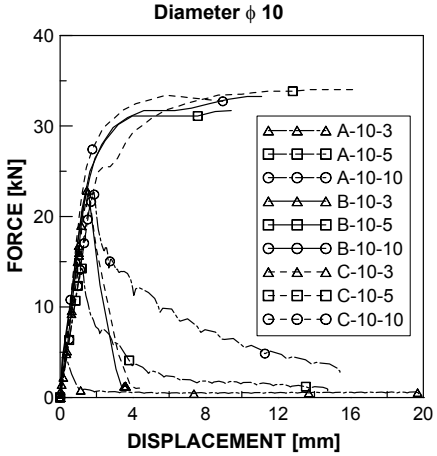

Figure 4: Bar diameter 10 mm. Influence of the embedment length and of the stone type on the failure mechanism.

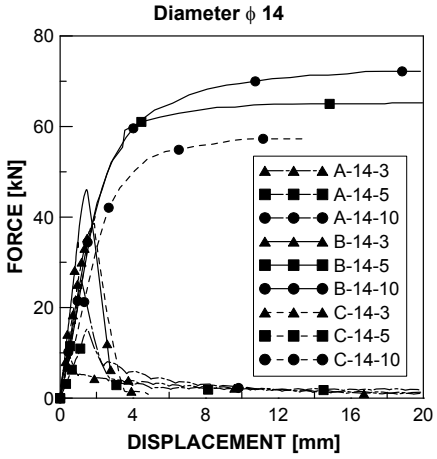

Figure 5: Bar diameter 14 mm. Influence of the embedment length and of the stone type on the failure mechanism.

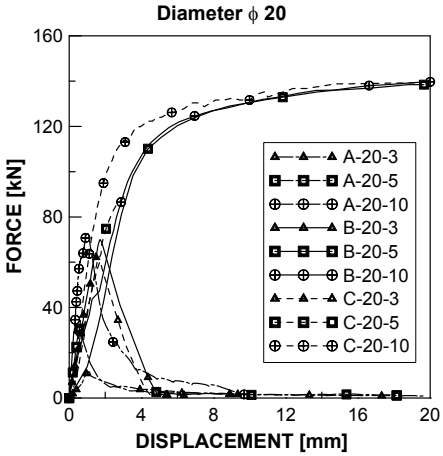

Figure 6: Bar diameter 20 mm. Influence of the embedment length and of the stone type on the failure mechanism.

THEORETICAL MODEL FOR THE PREDICTIONS OF THE PULL-OUT STRENGTH OF CHEMICAL ANCHORS

A number of studies exist in the literature concerning the calculation of the chemical anchor tensile load for different failure patterns. However, they are all referred to concrete. These models are based on the transfer of the applied load from the steel anchored element, through the adhesive layer, to the concrete along the entire bonded surface. They also account for the proximity of the anchor to the support edge and for the spacing in group anchors.

The tensile failure load of individual chemical anchors is usually calculated as a function of the depth of the anchor.

Cook, et al. [3] conducted a comprehensive investigation of more than 1000 tests with twenty types of adhesive products. According to this study, the parameters that affect the resistance of a chemical anchor are: adhesive strength; compressive strength of concrete; hole cleaning; humidity of the hole; high temperatures and creep; charging time. The possible failure mechanisms can be summarized as it follows:

1. if the embedment depth is very small, a concrete cone failure occurs.
2. if the depth of the anchor is greater we can have: a combined mechanism, given by a shallow concrete cone failure with sliding at the adhesive/concrete interface below the cone; a combined mechanism, given by a shallow concrete cone failure with sliding at the rod/adhesive interface below the cone; a combined mechanism, given by a concrete cone failure with sliding at the adhesive/concrete interface in the upper part of the anchor and sliding at the rod/adhesive interface in the lower part.
3. if the embedment depth is very high, the anchor is so resistant that the failure occurs for breakage of the steel bar.

The minimum depth for obtaining the rupture of the bar represents the embedment length of the anchor, also depending on the properties of steel and resin. The theoretical models proposed in the literature and reported in Table 2 have been applied to the materials under investigation for testing the possibility of their applications also in the case of natural rocks.

Model 1 is an *elastic bond-stress model* addressing the compatibility relationships between concrete, bonding agent and threaded rod. Model 2 is a *uniform bond-stress model* predicting the capacity of the anchor as a function of the uniform failure stress τ_0. Model 3 is a *uniform bond-stress model with real resistance of adhesive* in which the bond area effect is represented by an additional modification factor ψ_b. Model 4 is a *bond models neglecting the shallow concrete cone*, in which the effective embedment length is equal to the actual embedment length minus 3 times the diameter, to account for the shallow concrete cone. Models 5 and 6 are *combined cone-bond models*: model 5 is *combined concrete cone/ bond model uniform*; model 6 is *combined concrete cone / bond model elastic*. Models 7 and 8 are *interface bond model*: model 7 is based on the sliding at the *adhesive/concrete interface*; model 8 is based on the sliding at the *steel/adhesive interface*. Model 9 is a *concrete cone model*.

Model	Author	Ultimate axial force
1	Doerr er al. [8]	$N_u = \tau_{\max}\pi d_0\left(\frac{\sqrt{d_0}}{\lambda'}\tanh\frac{\lambda' h_{ef}}{\sqrt{d_0}}\right)$
2	McVay et al. (1996) [9]	$N_u = \tau_0\pi d_0 h_{ef}$
3	Nilson (1972) [1]	$N_u = \tau_0\pi d_0\Psi_b\Psi_c$
4	Cook et al. (1998) [10]	$N_u = \tau_0\ \pi d\left(h_{ef} - 3d\right)$
5	Cook et al. (1993) [11]	$N_u = 0.92h_{ef}^2\sqrt{f'} + \tau_0\pi d_0 h_{ef}$
6	Cook (1993) [2]	$N_u = 0.92h_{ef}^2\sqrt{f'} + \tau_{\max}\pi d_0\left(\frac{d_0}{\lambda'}\tan\frac{\lambda'\left(h_{ef} - h_{cone}\right)}{\sqrt{d_0}}\right)$
7	Marti (1993) [12]	$N_u = \tau_0\pi d h_{ef}$
8	Marti (1993) [12]	$N_u = \tau_0\pi d h_{ef}\sqrt{\frac{f_c}{f_{c,bw}}}$
9	Eligehausen et al. (1984) [6]	$N_u = 0.92h_{ef}^2\sqrt{f'}$

Table 2: Theoretical concrete models for the prediction of the ultimate anchor strength.

The following symbols enter the theoretical formulas in Table 2:

N_u pull-out force
d_0 hole diameter
d anchor diameter
τ_0 uniform bond stress
τ_{max} maximum bond stress for adhesive anchor
h_{ef} anchor embedment length
Ψ_b modification factor for bond area
Ψ_c modification factor for concrete strength
h_{cone} depth of cone, depending on τ_0, d_0, h_{ef}, f' as in [2]
f' concrete compressive strength measured with standard cylinders
$\lambda' = \sqrt{\frac{4G}{tE}}$ experimentally determined elastic constant that is dependent on shear stiffness G of the adhesive/concrete system , on the axial stiffness E of the threaded rod and on the thickness t of the adhesive layer

Theoretical models from 1 to 9 have been applied merely considering the stones material parameters in place of concrete parameters and the anchor embedment length and diameters in previous section. The maximum bond stress τ_{max} was taken equal to the tensile strength of the stone (assumed equal to one tenth of compressive strength in Table 1), the uniform bond stress τ_0 equal to 0.85 τ_{max}, $\Psi_b = \Psi_c = 1.0$.
Data in Fig. 7, 8 and 9 show the predictions for fixed stone type, by varying the rod diameter and the embedment length. In the columns labeled N_u all the predicted values exceeding the theoretical yield force (equal to 35,3 kN, 69,3 kN and 141,4 kN for steel rods with nominal diameter equal to 10 mm, 14 mm and 20 mm, respectively) are meaningless, because the yielding precedes the mechanism. The corresponding cells in the tables are highlighted. Columns labeled as "error" report the relative error w.r.t. the experimental data. Rows "Experimental" report, on the right of the pull-out force value, the crisis mode, so that it can be compared with the crisis mode defined by each theoretical model. Generally, three main mechanism were experimentally observed: 1) formation of a shallow stone cone with sliding at the stone/resin interface below the cone (Fig. 3(a)); 2) stone cone (Fig. 3(b,c)); 3) yielding of the steel rod (Fig. 2). More details are given in [7].
The only suitable model for basalt anchor results Model 6, combining an elastic bond-stress model with a concrete cone failure model. On the basis of the error value, in the case of limestone and sandstone the suitable model is Model 7 for L=3ϕ and ϕ =10-14 mm. However, it considers the sliding at the resin/stone interface, while the experimental crisis appeared as stone cone. Model 7 is the only adequate for sandstone in the case L=5ϕ, ϕ =20mm, but no sliding generally appeared in the experimental tests. In the case L=5ϕ and L=10ϕ a uniform trend cannot be recovered for sandstone and limestone. As a general comment, from the analysis of data in Fig. 7-9, it is evident that a single Model able to predict the behavior either for a selected material or for an assigned rod diameter and specific embedment depth, cannot be identified.
Moreover, the comparison of the results obtained by means of the application of theoretical models from 1 to 9 and the experimental data shows that the theoretical formulas can be applied to natural stones only if the mechanical characteristics of the stone are quite similar to the ones of a normal concrete for construction, with values of the rupture stress in compression between 20.0-50.0 MPa, as in the case of sandstone. On the contrary, they became useless and meaningless when the breakage of the steel bar precedes the other mechanisms 1-9. In this case the theoretical prediction of the rod rupture value can be considered exact when compared with the experimental one.

	Etna basalt							Etna basalt							Etna basalt						
	10							14							20						
	3Φ		5Φ		10Φ			3Φ		5Φ		10Φ			3Φ		5Φ		10Φ		
	Nu [kN]	error [%]	Nu [kN]	error [%]	Nu [kN]	error [%]		Nu [kN]	error [%]	Nu [kN]	error [%]	Nu [kN]	error [%]		Nu [kN]	error [%]	Nu [kN]	error [%]	Nu [kN]	error [%]	
Model 1	5.6	77.8%	5.6	83.5%	5.6	83.3%	Model 1	8.5	81.5%	8.5	87.6%	8.5	88.2%	Model 1	13.6	85.0%	13.6	90.4%	13.6	90.5%	
Model 2	59.4	135.2%	99.0	190.5%	197.9	489.2%	Model 2	106.9	131.9%	178.1	159.9%	356.3	393.2%	Model 2	203.6	124.7%	339.3	140.3%	678.6	375.3%	
Model 3	65.6	160.0%	106.1	211.4%	203.5	505.8%	Model 3	113.4	146.2%	183.3	167.5%	351.8	387.0%	Model 3	207.0	128.5%	334.6	137.0%	641.9	349.7%	
Model 4	0.0	100.0%	31.4	7.8%	110.0	227.3%	Model 4	0.0	100.0%	61.6	10.2%	215.5	198.4%	Model 4	0.0	100.0%	125.7	11.0%	439.8	208.1%	
Model 5	11.8	53.4%	51.4	50.8%	150.3	347.5%	Model 5	28.2	38.8%	99.4	45.1%	277.6	284.3%	Model 5	63.7	29.7%	199.4	41.2%	538.7	277.3%	
Model 6	24.1	4.4%	57.0	67.5%	211.3	529.1%	Model 6	44.8	2.7%	109.3	59.5%	411.7	470.0%	Model 6	87.7	3.3%	219.3	55.3%	836.5	485.9%	
Model 7	47.1	86.7%	78.5	130.6%	157.1	367.6%	Model 7	92.4	100.4%	153.9	124.6%	307.9	326.2%	Model 7	188.5	108.0%	314.2	122.5%	628.3	340.1%	
Model 8	59.4	135.2%	99.0	190.5%	197.9	489.2%	Model 8	106.9	131.9%	178.1	159.9%	356.3	393.2%	Model 8	203.6	124.7%	339.3	140.3%	678.6	375.3%	
Model 9	18.5	26.6%	51.4	51.0%	205.7	512.4%	Model 9	36.3	21.2%	100.8	47.0%	403.2	458.2%	Model 9	74.1	18.3%	205.7	45.7%	822.9	476.4%	
Experimental	25.2	shallow cone	34.1	yielding rod	33.6	yielding rod	Experimental	46.1	shallow cone	68.6	yielding rod	72.2	yielding rod	Experimental	90.6	shallow cone	141.2	yielding rod	142.8	yielding rod	

Figure 7: Etna basalt. Percentage error on the theoretical pull-out force estimation.

	Floresta limestone							Floresta limestone							Floresta limestone						
	10							14							20						
	3Φ		5Φ		10Φ			3Φ		5Φ		10Φ			3Φ		5Φ		10Φ		
	Nu [kN]	error [%]	Nu [kN]	error [%]	Nu [kN]	error [%]		Nu [kN]	error [%]	Nu [kN]	error [%]	Nu [kN]	error [%]		Nu [kN]	error [%]	Nu [kN]	error [%]	Nu [kN]	error [%]	
Model 1	2.6	88.4%	2.6	92.5%	2.6	92.4%	Model 1	3.9	89.8%	3.9	90.2%	3.9	93.2%	Model 1	6.3	89.7%	6.3	93.8%	6.3	95.6%	
Model 2	26.4	18.3%	44.0	27.9%	88.0	159.9%	Model 2	47.5	23.0%	79.2	97.5%	158.3	172.9%	Model 2	90.5	49.7%	150.8	49.3%	301.6	114.0%	
Model 3	29.2	30.7%	47.1	37.1%	90.4	167.2%	Model 3	50.4	30.6%	81.5	103.3%	156.3	169.4%	Model 3	92.0	52.2%	148.7	47.2%	285.3	102.4%	
Model 4	0.0	100.0%	14.5	58.0%	50.6	49.5%	Model 4	0.0	100.0%	28.3	29.3%	99.1	70.8%	Model 4	0.0	100.0%	57.8	42.8%	202.3	43.5%	
Model 5	12.5	43.9%	30.1	12.4%	74.1	119.0%	Model 5	24.6	36.3%	56.2	40.3%	135.4	133.4%	Model 5	49.7	17.7%	110.1	8.9%	260.8	85.1%	
Model 6	15.1	32.2%	37.5	8.9%	142.1	319.9%	Model 6	28.5	26.1%	72.3	80.3%	277.4	378.0%	Model 6	56.5	6.6%	145.8	44.3%	564.4	300.4%	
Model 7	21.7	2.8%	36.1	5.1%	72.3	113.5%	Model 7	42.5	10.0%	70.8	76.6%	141.6	144.1%	Model 7	86.7	43.5%	144.5	43.0%	289.0	105.1%	
Model 8	26.4	18.3%	44.0	27.9%	88.0	159.9%	Model 8	47.5	23.0%	79.2	97.5%	158.3	172.9%	Model 8	90.5	49.7%	150.8	49.3%	301.6	114.0%	
Model 9	12.6	43.7%	34.9	1.4%	139.5	312.3%	Model 9	24.6	36.3%	68.4	70.5%	273.5	371.3%	Model 9	50.2	16.9%	139.5	38.1%	558.1	296.0%	
Experimental	22.3	shallow cone	34.4	yielding rod	33.8	yielding rod	Experimental	38.6	shallow cone	40.1	shallow cone	58.0	yielding rod	Experimental	60.4	shallow cone	101.0	yielding rod	141.0	yielding rod	

Figure 8: Floresta limestone. Percentage error on the theoretical pull-out force estimation.

	Palagonia sandstone							Palagonia sandstone							Palagonia sandstone						
	10							14							20						
	3Φ		5Φ		10Φ			3Φ		5Φ		10Φ			3Φ		5Φ		10Φ		
	Nu [kN]	error [%]	Nu [kN]	error [%]	Nu [kN]	error [%]		Nu [kN]	error [%]	Nu [kN]	error [%]	Nu [kN]	error [%]		Nu [kN]	error [%]	Nu [kN]	error [%]	Nu [kN]	error [%]	
Model 1	0.5	88.2%	0.5	96.2%	0.5	96.8%	Model 1	0.8	91.2%	0.8	94.6%	0.8	96.9%	Model 1	1.3	88.8%	1.3	95.7%	1.3	98.2%	
Model 2	5.7	24.5%	9.5	33.3%	19.0	11.8%	Model 2	10.3	10.8%	17.1	12.5%	34.2	31.3%	Model 2	19.5	67.3%	32.6	6.2%	65.1	10.8%	
Model 3	6.3	37.5%	10.2	28.5%	19.5	14.9%	Model 3	10.9	17.6%	17.6	15.8%	33.8	29.7%	Model 3	19.9	70.1%	32.1	4.8%	61.6	15.6%	
Model 4	0.0	100.0%	3.0	78.8%	10.6	37.9%	Model 4	0.0	100.0%	5.9	61.1%	20.7	20.5%	Model 4	0.0	100.0%	12.1	60.7%	42.2	42.2%	
Model 5	3.5	23.4%	7.3	48.7%	16.8	1.1%	Model 5	6.6	28.4%	13.5	11.4%	30.6	17.4%	Model 5	13.1	12.1%	26.1	14.8%	58.7	19.6%	
Model 6	4.2	7.4%	10.8	24.0%	41.7	145.2%	Model 6	8.1	12.8%	21.0	38.0%	81.5	212.8%	Model 6	16.1	38.0%	42.4	38.4%	165.9	127.2%	
Model 7	4.5	1.2%	7.5	47.1%	15.1	11.3%	Model 7	8.9	4.2%	14.8	2.8%	29.6	13.5%	Model 7	18.1	54.9%	30.2	1.6%	60.3	17.4%	
Model 8	5.7	24.5%	9.5	33.3%	19.0	11.8%	Model 8	10.3	10.8%	17.1	12.5%	34.2	31.3%	Model 8	19.5	67.3%	32.6	6.2%	65.1	10.8%	
Model 9	3.7	19.2%	10.3	27.8%	41.1	142.0%	Model 9	7.3	21.6%	20.2	32.6%	80.6	209.7%	Model 9	14.8	26.8%	41.1	34.2%	164.6	125.4%	
Experimental	4.6	shallow cone	14.2	shallow cone	17.0	shallow cone	Experimental	9.3	shallow cone	15.2	shallow cone	26.0	shallow cone	Experimental	11.7	shallow cone	30.7	shallow cone	73.0	shallow cone	

Figure 9: Palagonia sandstone. Percentage error on the theoretical pull-out force estimation.

NUMERICAL PREDICTION OF THE PULL-OUT STRENGTH

The comparison between the theoretical results obtained by means of the application of concrete models and the experimental data suggests that two way may be covered. The development of new theoretical formulations, whose formulas fit the experimental results, or the prediction of the pull-out strength by means of numerical analysis. The task at hand, beyond the scientific interest due to the possible application of a lot of advanced models to achieve the failure prediction of the rupture mechanism and of the bearing capacity, is especially a practical problem encountered by technicians and engineers. They denounce the lack of information about the necessary embedment depth for the considered materials. Only the suggestion of the resin producer is available and there isn't any normative recommendation. The design and usage of embedment depth different from the one suggested by the resin producer, that results oversized for those materials having low compressive strength, must be widely justified to the competent authority. For this purpose the engineers usually make use of software for structural analysis, in which only few constitutive model are implemented for modeling brittle materials like rocks. Very often just geotechnical material models are the possible choice, sometimes limited to specific stress states. Three widespread professional software for structural analysis [14-16] were studied to understand the possible way for modeling the experiments. When present, the possible inelastic constitutive models available for the stone behaviour were Drucker Prager and Mohr-Coulomb criteria. No specific capability for modeling the stone-resin and rod-resin interface behavior was found.

With the aim of understanding the reliability of these numerical simulations, provided the exact material parameters have been assigned, the experimental tests described in the previous section were numerically reproduced.

A first set of simulations was built with the commercial software Adina (version 8.8), because this software implements in addition to *Mohr-Coulomb* and *Drucker-Prager* models available in [14-16], the *Microplane Concrete* model [16].

All the eighty-one experimental tests previously described were numerically reproduced. Thanks to the polar symmetry of the geometrical and mechanical characteristics of the problem, the numerical simulations were carried out under the axis-symmetric stress regime. Therefore, just a 1 radian central angle portion of the system was discretised. Roller supports allowing vertical displacements were entered along the bar axis and roller supports allowing horizontal displacements were entered along the base of the model.

The loading condition consisted in the self weight and in imposed vertical displacement at the top end of the steel bar.

The friction angle and the cohesion coefficient, entering the Mohr-Coulomb and Drucker-Prager models of the rock, were evaluated in terms of the tensile and compressive strength of the materials. Tensile strength was assumed equal to

one tenth of compressive strength. The mechanical properties of the rocks in Table 1 were used with Poisson ratio equal to 0.25. The parameters characterising the Microplane Concrete Model were accordingly calculated.
The steel bar was modelled according to a bilinear constitutive law with hardening (Young Modulus 206000 MPa, yield stress 400 MPa, hardening modulus 100 MPa, Poisson ratio 0.3). The resin was hypothesised as linear elastic with the material properties specified by the manufacturer.
The analyses provided a reliable value of the ultimate strength, except in the case of test B-10-3 for which a rod failure was predicted by the numerical simulation, while the effective crisis was characterized by a stone cone mechanism. However, a stiffer behavior of the model affects the simulations of pull-out tests with the lower embedment length L=3ϕ, as it can be seen for instance in Fig. 10 for all the three models. The Microplane Concrete Model was often affected by the loss of convergence well before the peak load. It has been observed that the pathologic behavior of the models, when considering the shorter embedment length L=3ϕ, can be ascribed to the hypothesis of axis-symmetric regime.

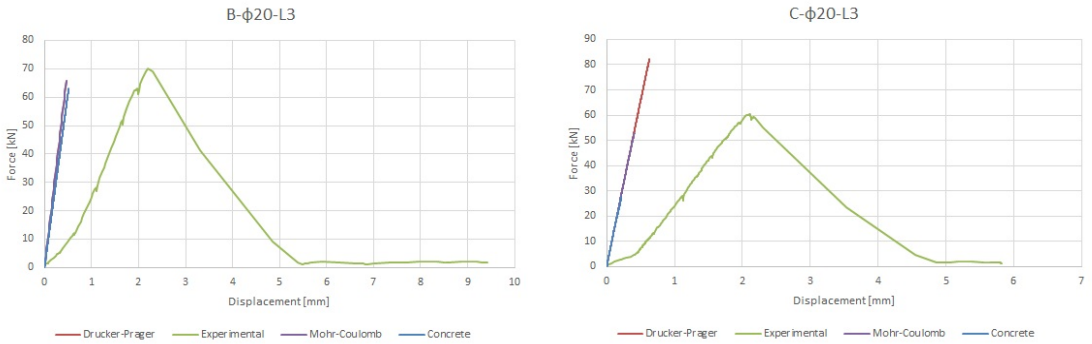

Figure 10: Basalt (a) and Limestone (b) predictions for ϕ=20 mm, L=3ϕ.

This conclusion was confirmed by two additional simulations of test B-10-3. The first, in plain strain regime, gave the same inaccuracy on the initial stiffness; the second, carried out in plane stress, using for simplicity the Von Mises constitutive model under the hypothesis of elastic-plastic behaviour without hardening, showed the right prediction of the initial stiffness (see Fig. 11). That is, in the case of very short embedment length, a stress state accounting for confinement actions is not adequate in reproducing the physical behavior, in agreement with what observed in [9].
For basalt and limestone the peak load prediction was really accurate for L=5 ϕ and L=10 ϕ, the crisis being related to the yielding of the steel bar. In this situation the bilinear elastic-plastic criterion of the steel rod rules the problem. Therefore, the error on the solution is very low. For sandstone the stone cone crisis was almost correctly predicted, as well as the pull-out strength and stiffness of the system, as it can be observed in Fig. 12.
A uniform trend in the reliability of the numerical prediction was not recovered. The reason can be ascribed to mixed failure mechanisms, due to unpredictable physical and mechanical phenomena arising during the physical cracking process and also caused by imperfect bonding, whose prediction by means of numerical simulation is not feasible.

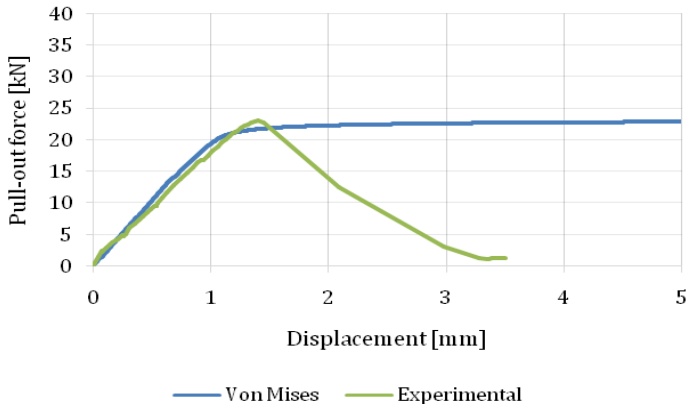

Figure 11: Von Mises plane stress elastic-plastic simulation of test B-10-3.

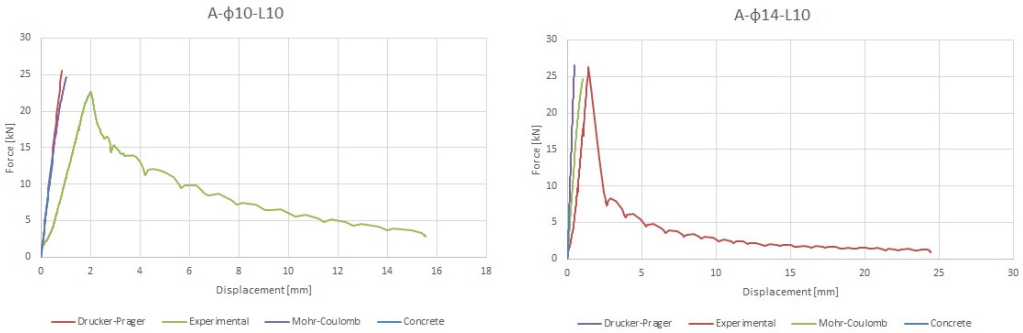

Figure 12: Sandstone failure prediction ϕ=10 mm and ϕ=14 mm, L=10ϕ.

Despite the inaccurate determination of the limit strength, the limit value of the embedment depth, separating the rock failure from the steel failure is correctly identified. Therefore the determination of the necessary embedment length to obtain the road breakage can even be made by using professional software.
On the contrary, only appropriate numerical simulations can reproduce the crisis mechanism for each embedment length, provided that the materials properties are correctly identified.
Therefore, a second set of simulations was built with two different advanced numerical codes, able to reproduce the complete evolution of the cracking process. The same material parameters utilised in previous simulations were adopted.
In the first case the study of the post-critic behaviour of the stone was made by means of a numerical model based on the Strong Discontinuity Approach (SDA) and proposed in [18-20]. Cracks are numerically simulated by a jump in the displacement field, that can be physically identified with the discontinuity surface that arises, for instance, in the failure mechanism previously described with development of a cone in the rock. The opening of cracks is ruled by the bilinear cohesive fracture activation function in Fig. 13, defined by the activation traction of the rock f_0, the softening moduli $H_{S,1}$ and $H_{S,2}$ and the limit crack opening w_{cr}.

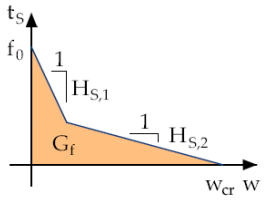

Interface
f_0=20 MPa
$H_{S,1}$=-66.6 MPa/mm
$H_{S,2}$=-6.0 MPa/mm
w_{cr}=0.45 mm

Bulk
E=50000 MPa
ν=0.2

Steel rod
E= 206000 MPa
f_y=400 MPa
ν=0.3

Figure 13: Cohesive fracture criterion.

The continuum behaves linearly elastic. The steel rod constitutive model is the elastic- plastic one with yield stress f_y. The values of the parameters are given in the picture. The numerical algorithm falls in the context of the Finite Elements with Embedded Discontinuity. It was implemented in the original code FracSDA8 developed in [21].
The model has been applied to the analysis of the post-installed adhesive anchors under investigation. The simulation of test B-10-3, that always gave bad results by using standard software, was performed, under the hypothesis of plane stress. In fact, in the test in question, the embedment depth is equal to 3 times the diameter, i.e. 3 cm. Therefore, the anchoring is so near the surface of the stone block that the confinement characterising axis-symmetric stress states is negligible and the plane stress state hypothesis is admissible [7].
The model accurately predicts the initial activation of the failure, that starts for detachment of the bottom end of the bar, under a preponderant tensile stress state in that area. Then, failure progresses and develops along a shear band, with angle equal about to the friction angle of the stone. The peak load given by the numerical analysis is in good agreement with the experimental one, as it is shown in Fig. 14.
In the second case, the simulations were built by using the commercial software Midas FEA [22]. Unlike the previously analysed commercial software [14-16], it implements seven different interface models. Specifically, the bond-slip model was used in the simulations, coupled to a Mohr-Coulomb criterion for the description of the stone behavior. Once again the steel bar was modelled according to a bilinear constitutive law with hardening. The bond-slip constitutive law was used for modeling the behavior at the resin-stone interface, while a perfect adhesion between the resin and the rod was

assumed, on the basis of the experimental evidence. The cubic function in Fig. 15, depending only on two constitutive parameters, was selected.

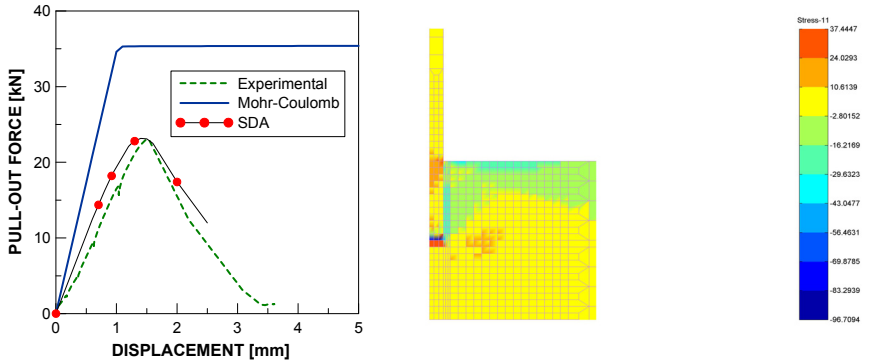

Figure 14: SDA simulation by code FracSDA8 of test B-10-3. Pull-out force and stress distribution at the peak load.

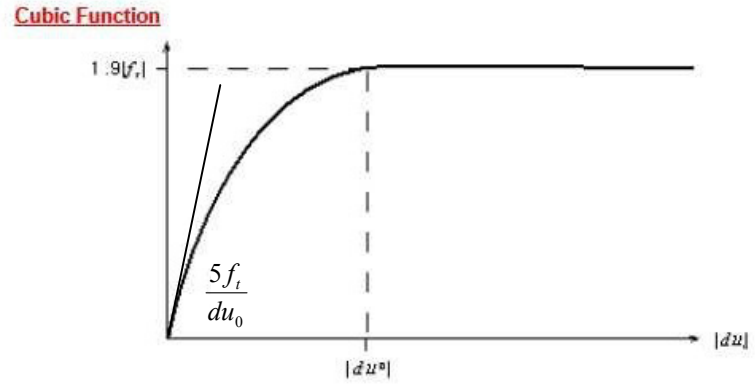

$$f_t = \begin{cases} f_t\left(5\left(\frac{du_t}{du^0}\right) - 4.5\left(\frac{du_t}{du^0}\right)^2 + 1.4\left(\frac{du_t}{du^0}\right)^3\right) & if \quad 0 \le du_t \le du^0 \\ 1.9\, f_t & if \quad du_t \ge du^0 \end{cases}$$

Figure 15: Bond slip model. Interface stress versus shear slip.

Table 3 reports the parameters value assumed in the calculations.
The predictions were once again accurate, both in the estimation of the pull-out strength and in the prediction of the failure mechanism.
For example, in Fig. 16 the results concerning test B-14-10 are reported. The maximum value of parameters in Table 3 were used. The steel bar rupture and the corresponding anchor strength are correctly reproduced, as it can be observed by the comparison between pictures 16 and 5.

	Initial Tangent Stiffness $5 f_t / du_0$ [N/mm³]	Constant $1.9 f_t$ [N/mm²]	Shear Slip du_0 [mm]
Basalt	50000	35 ÷ 50	0.1 ÷ 1
Limestone	20000	15	0.1 ÷ 1
Sandstone	11000	2 ÷ 5	0.1 ÷ 1

Table 3: Bond slip model parameters

Figure 17 shows the evolution of the failure mechanism in term of maximum principal stress for test A-10-5, while in Fig. 18(a) the crisis mechanism of sample B-10-3-2 at the pull-out strength is compared with the experimental one. Fig. 18(b) represent the corresponding plastic flag. The percentage error in the pull-out strength estimation was always in the order of 5%.

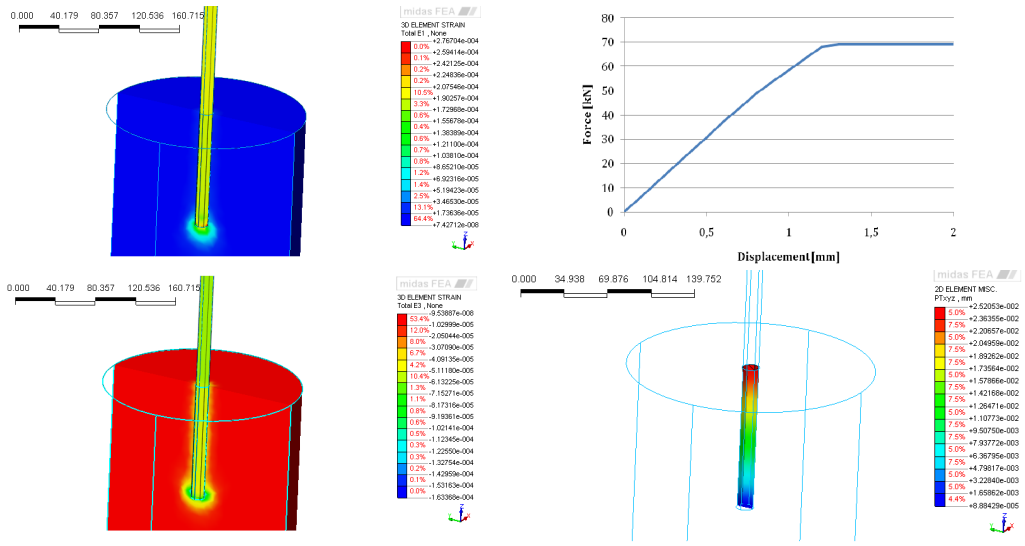

Figure 16: Test B-14-10. Steel rod failure.

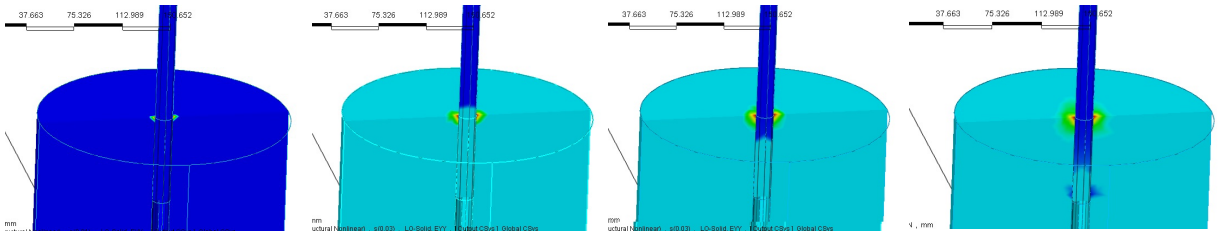

Figure 17: Test A-10-5. Evolution of the radial stress

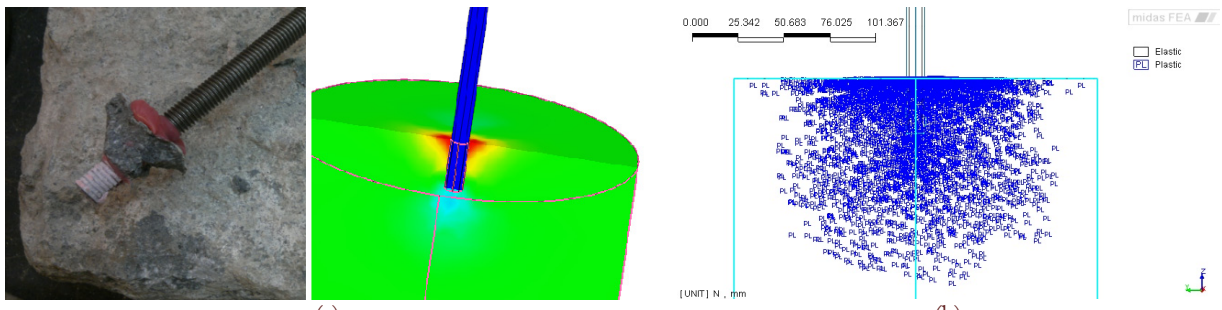

(a) (b)

Figure 18: Test B-10-3. Radial principal strain (a) and plastic flag at the peak load (b).

CONCLUSIONS

The numerical prediction of the failure mechanism of anchor systems chemically bonded in natural stone requires sophisticated computational tools for capturing all the evolution of the crisis process, as for instance those used in the present paper or many other, equally rich, often implemented in advanced commercial F.E. codes.
The entire phenomenon is actually complex due to the presence of three different material characterised by quite different mechanical properties. Professional software, generally used by technicians in the field of construction and by the

engineers engaged in structural analysis, are often not sufficiently equipped with advanced mechanical formulation or constitutive models. A critical capability of the designer is needed to understand the limit of the simulation. Furthermore the lack of experimental data concerning the minimum embedment length in the investigated materials implies that engineers apply the recommendation of the resin manufacturer, often oversized with respect to the real anchor depth. Therefore a database covering the main lithological types presents in each territorial area should be built.
The numerical simulations developed in the paper illustrate how a bad modeling can produce really approximated results, eventually useful just in the estimation of limit value of the embedment depth separating the yielding of the steel bar from the localised fracture of the stone support. The results of these numerical test are indeed in agreement with the experimental evidence in term of ultimate strength only in the case of large embedment depth, in basalt and limestone, when the failure is depending on the yield stress of the rod. In that situations the elastic-plastic behaviour of the steel rod rules the problem and the numerical prediction is reliable. On the contrary, in the case of stone support with scarce mechanical properties or for very short embedment length the crisis arises with the development of a rupture cone, that remain perfectly bonded to the rod, for all its embedded length or only in the upper portion of it. The simulation of such mechanism is a difficult task, requiring specific tools and the opportune characterization of the constitutive laws ruling the behavior of the anchor constituents. Only following this way the correct prediction of the anchor strength and fracture phenomenon can be effectively pursued.

REFERENCES

[1] Nilson, A. H., Internal Measurement of Bond Slip, ACI Structural Journal, 69 (1972) 439-441.
[2] Cook, R. A., Behavior of chemically bonded anchors, Journal of Structural Engineering, 119 (1993) 2744-2762.
[3] Cook, R. A., Konz, R. C., Factors Influencing Bond Strength of Adhesive Anchors, ACI Structural Journal, 98 (2001) 76-86.
[4] Colak, A., Parametric study of factors affecting the pull-out strength of steel rods bonded into precast concrete panels, International Journal of Adhesion & Adhesives, 21 (2001) 487-493.
[5] Bickel, T. S., Shaikh, A. Fattah, Shear Strength of Adhesive Anchors, PCI Journal, Sept-Oct (2002) 92-102.
[6] Eligehausen, R., Cook, R. A., Appl, J., Behavior and Design of Adhesive Bonded Anchors, ACI Structural Journal, 103 (2006) 822-831.
[7] Contrafatto, L., Cosenza, R., Experimental behaviour of post-installed adhesive anchors in natural stone, to appear, Construction and Building Materials, (2014).
[8] Doerr, G. T., Cook, R. A., Klingner, R. E., Adhesive Anchors: Behaviour and Spacing Requirements, University of Texas, Austin, Research Report n. 1126-2 (1989)
[9] McVay, M., Cook, R., Krishnamurthy, K., Pullout Simulation of Postinstalled Chemically Bonded Anchors, J. Struct. Eng., 122 (1996) 1016-1024.
[10] Cook, R. A., Kunz, J., Fuchs, W., Konz, R. C., Behavior and Design of single adhesive anchors ander tensile load in uncracked concrete, ACI Structural Journal, 95 (1998) 9-26.
[11] Cook, R. A., Doerr, G. T., Klingner, R. E., Bond stress model for design adhesive anchors, ACI Structural Journal, 90 (1993) 514-524.
[12] Marti, P., Anchoring of Concrete Reinforcement Using HIT-HY 150, Hilti Development Corporation, Technical Report n. 93.327-1 (1993).
[13] Eligehausen, R., Mallee, R., Rehm, G., Befestigungen mit Verbundankern (Fastenings with bonded anchors, Betomverk + FertigteilTechnik, 10 (1984) 686-692.
[14] SAP2000, http://www.csi-italia.eu/software/sap2000/, (2014).
[15] PRO_SAP, http://www.2si.it/, (2014).
[16] Straus7, http://www.enginsoft.it/software/straus/index.html, (2014).
[17] Bazant, Z. P., Prat, P. C., Microplane model for brittle-plastic material. I: Theory. II: Verification., J. Engrg. Mech., 114(1988) 1672-1699
[18] Contrafatto, L., Cuomo, M., Di Venti, G.T., Finite elements with non homogeneous embedded discontinuities, European Congress on Computational Methods in Applied Sciences and Engineering, (2012) 9152-9171.
[19] Contrafatto, L., Cuomo, M. , Fazio, F., An enriched finite element for crack opening and rebar slip in reinforced concrete members, International Journal of Fracture, 178 (2012) 33-50.
[20] Cuomo, M., Contrafatto, L., Greco, L., A variational model based on isogeometric interpolation for the analysis of cracked bodies, International Journal of Engineering Science 80 (2014) 173–188.

[21] Di Venti, G. T., Modellazione numerica della nascita e dello sviluppo di interfacce mediante il metodo delle discontinuità forti intraelemento, Università di Catania, Dipartimento di Ingegneria Civile e Ambientale, PhD Thesis, (2012).
[22] Midas FEA, http://www.cspfea.net/midas_fea.php, (2014).